# MIMO DWDM System Using Uncooled DFB Lasers With Adaptive Laser Bias Control and Postphotodetection Crosstalk Cancellation

Jiannan Zhu, Jonathan D. Ingham, *Member, IEEE*, Johannes Benedikt von Lindeiner, Adrian Wonfor, *Member, IEEE*, Richard V. Penty, *Senior Member, IEEE*, and Ian H. White, *Fellow, IEEE*

***Abstract*—A proof-of-principle demonstration of a multiple input-multiple output (MIMO) dense wavelength division multiplexing (DWDM) system is reported. It uses standard uncooled distributed feedback lasers with intensity modulation-direction detection (IM-DD), in which the temperature of each laser is allowed to drift independently within a 50 °C temperature range. A feedback-based laser bias control algorithm is introduced to guarantee acceptable wavelength spacing and a postphotodetection minimum mean square error decoder is applied to cancel the interchannel crosstalk. The relative sensitivity of the MIMO receiver in both a random laser temperature drift scenario and a worst-case scenario are investigated by simulations in MATLAB. Experimental results for a 40-channel × 12.5 Gb/s DWDM system transmitting over 28 km of single-mode fiber with worst possible wavelength distribution prove the feasibility of the technique.**

***Index Terms*—Energy consumption, multiple input multiple output, wavelength division multiplexing.**

## I. Introduction

With the rapid growth of Internet traffic [1], WDM has been proven to be a powerful technique in expanding the transmission capacity [2], [3] of long-haul transmission links [4], [5], metro area networks [6], [7] and optical access networks [8], [9]. However, owing to narrow wavelength spacing, current WDM systems demand higher wavelength accuracy and stability against environmental changes to achieve low crosstalk operation. These requirements typically need the transceivers to feature wavelength monitoring or locking units and thermo electric coolers (TECs), both of which lead to excessive cost, power consumption and system complexity [10]. With the growing awareness of the enormous power consumption in the ICT industry [11]–[13], approaches for low cost WDM systems have been extensively studied over the last few years [14], [15]. As described below, most of this research falls into three categories: coarse WDM (CWDM) systems with greater wavelength spacing, uncooled transmitter design and a recently emerged method of introducing a MIMO setup in the receiver.

The CWDM approach uses a larger channel spacing to achieve a large allowable wavelength deviation [16]. However, this is at the cost of significantly decreased spectral efficiency and only a relatively few sub-channels can be supported in CWDM. Meanwhile, many designs for uncooled transmitters have been reported [17], [18]. These transmitters successfully eliminate the TECs without changing the wavelength spacing. However, not only do they need an extra control circuit or system to lock the emission wavelength but also the lasers need to be tunable lasers [19] or injection-locked vertical-cavity surface-emitting lasers [20], which are more complex than current lasers in use.

Recently, a novel uncooled DWDM system design has been reported [21], [22], in which the wavelengths are allowed to drift freely but all by the same extent and an IM-DD based MIMO receiver followed by an MMSE decoder is used to cancel the crosstalk. Unlike the other two approaches, this system still uses standard DFB lasers that are used in most current WDM systems. However, this system is vulnerable to the relative temperature (and hence wavelength) drift between adjacent channels. If the neighboring channels' wavelengths move close to each other, caused by the uneven temperature drift, the power penalty of the MMSE decoder will dramatically increase and eventually the system will fail.

In this paper, this limitation of the previous work has been overcome by introducing a feedback based laser bias control algorithm to adjust adaptively the channel spacing to ensure error free measurement. This design allows every individual uncooled laser's temperature to drift independently within a 50 °C range. The proposed MIMO setup including an arrayed waveguide grating (AWG) design is introduced in Section II. A detailed description of the second-stage laser bias control algorithm is shown in Section III. Section IV illustrates a comprehensive study of the system performance in different temperature scenarios by simulation. In Section V, an experiment of a 40 channel × 12.5 Gb/s DWDM system transmitting over 28 km of single mode fiber (SMF) with the worst possible wavelength distribution is successfully demonstrated.

## II. Principle of the MIMO DWDM System

In an uncooled WDM system, the laser emission wavelength can drift with temperature. Therefore, when using a conventional AWG, the signal may be lost due to the wavelength drift in the

Manuscript received November 29, 2013; revised March 31, 2014 and May 29, 2014; accepted June 23, 2014. Date of publication June 30, 2014; date of current version September 17, 2014. This work was supported by the Engineering and Physical Science Research Council for their financial support via the INTERNET project.

The authors are with the Centre for Photonic Systems, Department of Engineering, University of Cambridge, Cambridge, CB3 0FA, U.K. (e-mail: Jz333@cam.ac.uk; jdi21@cam.ac.uk; jbv22@cam.ac.uk; aw300@cam.ac.uk; rvp11@cam.ac.uk; ihw3@cam.ac.uk).

Color versions of one or more of the figures in this paper are available online at http://ieeexplore.ieee.org.

Digital Object Identifier 10.1109/JLT.2014.2334474

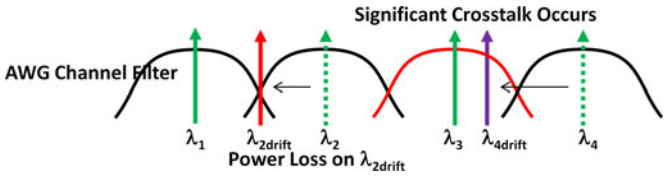


Fig. 1. Two issues caused by wavelength drift: power loss and crosstalk.

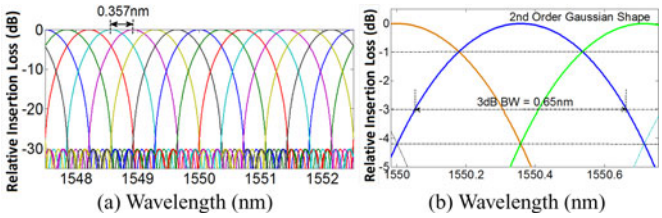


Fig. 2. (a) AWG with more receiver channels than transmitters. (b) The proposed AWG filter shape and specifications.

gaps between receiver channels. Furthermore, if one wavelength drifts towards the other channels, significant crosstalk occurs and the transmission will fail (see Fig. 1).

### A. MIMO WDM System

To avoid the power loss caused by the wavelength drift with temperature, we design a cyclic AWG with the number of receiver channels to be 2.8 times the number of transmitters (see Fig. 2(a)), which is chosen as the minimum receiver number that allows for a worst-case decoding penalty to be less than 5 dB. As the transmitters are set to have 1 nm nominal wavelength spacing, the receivers are therefore spaced by 0.36 nm. Each channel's response is of a Gaussian shape with a 3 dB bandwidth of 180% of the channel spacing (0.65 nm) and the cross point between adjacent channels is only $-1$ dB (Fig. 2(b)). This ensures that for any emission wavelength the signal will not be lost in the null between the conventional AWG channels.

In contrast to a system with a conventional AWG response where every output port only outputs the signal on a certain wavelength with very low crosstalk, the outputs from the AWG may comprise the signals from two or even more transmitters, which depend on the channel response and the source lasers' emission wavelengths. Assuming that the system is linear, equation (1) shows the expression of the combined output received by a PD from an individual AWG output port:

$$pd_x(t) = \{a_1, a_2, a_3, \ldots a_N\} \cdot \begin{Bmatrix} \text{input}_1(t) \\ \text{input}_2(t) \\ \ldots \\ \text{input}_N(t) \end{Bmatrix} \tag{1}$$

where $a_i (i = 1, 2, 3 \ldots, N)$ represents the channel's response to each input signal $\text{input}_i$ *(t)* $(i = 1, 2, 3, \ldots, N)$ and *N* is the total number of the inputs. Hence, the proposed AWG can be

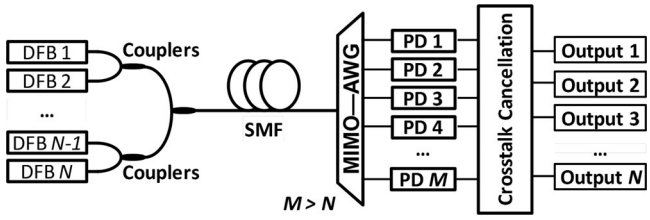


Fig. 3. The proposed MIMO-WDM system with *N* transmitters and *M*.

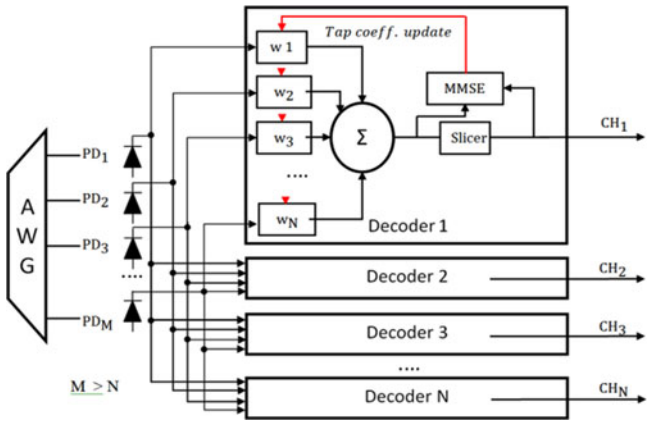


Fig. 4. Post-photodetection MMSE decoder array.

modeled using a transfer matrix:

$$\text{PD} = \begin{Bmatrix} pd_1 \\ pd_2 \\ \ldots \\ pd_M \end{Bmatrix} = \text{Awg}_{\text{Matrix}} \cdot \text{Input}$$

$$= \begin{Bmatrix} a_{11} & a_{12} & \ldots a_{1N} \\ a_{21} & a_{22} & \ldots a_{2N} \\ \ldots & \ldots & \ldots \ldots \\ a_{M1} a_{M2} & & \ldots a_{MN} \end{Bmatrix} \cdot \begin{Bmatrix} \text{input}_1(t) \\ \text{input}_2(t) \\ \ldots \\ \text{input}_N(t) \end{Bmatrix} \tag{2}$$

where *M* is the total number of output ports of the AWG and where $M > N$. Thus, by left-multiplying by a generalized inverse of the transfer matrix as shown in (3), we are able to cancel the crosstalk and recover the original signals:

$$\text{Input} = \text{AWG}^{-1} \cdot \text{PD}. \tag{3}$$

Fig. 3 shows the schematic diagram of a WDM system using the MIMO-AWG followed by a PD array and the crosstalk cancellation unit.

### B. MMSE Decoder

To implement this decoding process, we design a minimum mean square error (MMSE) decoder array. For each decoder, an unique tap $w_i$ is be assigned to each PD's output. These taps are calculated from an iterative MMSE process, which minimises the MSE between the sample sequence and the reference sequence. Finally, the signal is recovered by adding these weighted outputs from the PDs together (see Fig. 4).

The power penalty induced by this MMSE decoder results from two aspects: the residual crosstalk caused by the imperfect taps and the noise enhancement during the decoding process. The residual crosstalk can be suppressed to a negligible level by increasing the number of iterations in the MMSE process. The standard deviation of the thermal noise in the decoded signal can be calculated as

$$\sigma_{\mathrm{CH1}} = \sqrt{w_1^2\sigma_{\mathrm{PD1}}^2 + w_2^2\sigma_{\mathrm{PD2}}^2 + w_3^2\sigma_{\mathrm{PD3}}^2 + \cdots + w_M^2\sigma_{\mathrm{PDM}}^2} \tag{4}$$

where $\sigma_{\mathrm{PD}i}$ stands for the standard deviation of the thermal noise in photo-detector $i$ ($i = 1, 2, 3 \ldots M$) and $w_i$ is the tap assigned to its output. By assuming all PDs have the same noise level, we have

$$\sigma_{\mathrm{CH1}} = \sigma_{\mathrm{PD}}\sqrt{w_1^2 + w_2^2 + w_3^2 + \cdots + w_M^2}. \tag{5}$$

Equation (5) indicates that the noise figure of such an MMSE decoder is determined by the taps from the pseudo-inverse of the AWG transfer matrix. The electrical power consumption of this decoder depends on the total number of taps used for decoding all channels.

Table I lists individual component power consumptions for the proposed uncooled MIMO DWDM transceiver and a conventional DWDM transceiver. We assume both systems use standard DFB lasers modulated with 10 Gb/s NRZ signals. All the other components are identical except that the proposed system uses bias control and MIMO AWG and receivers, whilst the conventional system uses TECs and a regular AWG and receivers. It should be noticed that the bias control function contains only tens of lines of C code, which can be easily programmed into a micro controller which already exists in most DWDM transceiver modules. Besides, for the MIMO DWDM system, the updating of the taps at the receiver requires ADCs and some computations. However, due to the relatively slow temperature drift, the taps only need to be updated every few seconds. The calculations of this only take a few milliseconds and this can be done without interrupting the data signals. Thus, all decoders can share a single taps updating unit on different time slots. The results in Table I show that a MIMO DWDM system has a predicted power saving of 40%.

## III. Feedback Based Laser Bias Control Algorithm

Under most conditions, the signals can be recovered after crosstalk cancellation. However, when two or more channels drift too close to each other due to the changes in temperature, the MMSE decoder will fail owing to significant noise enhancement. In particular, it becomes theoretically impossible to decode the signals when two or more channels fully overlap at the same wavelength. Therefore, to avoid such a failure, in this paper we intentionally control the bias currents of the lasers to slightly move their emission wavelengths away from each other. The tuning process comprises three steps: wavelength determination, feedback, and laser bias tuning.

### A. Wavelength Determination

In the AWG, we have a set of channel filters whose centers are evenly distributed over the whole wavelength range. Therefore, through comparing the output powers from different channels, we can locate these wavelengths. This can be done by simply inspecting the numbers in the system transfer matrix.

As each tap corresponds to the power received by one receiver channel from a single transmitter, the emission wavelength from a single laser must be located between two central positions of the receivers with the largest and the second largest taps. Therefore, by comparing these two taps and the associated channel filter profile, we can locate the wavelength very accurately. Once we have this wavelength information for every channel, we can send it back to the transmitter to drive the bias control algorithm.

### B. Laser Bias Tuning Algorithm

Compared with the maximum wavelength drift within the given temperature range, laser bias tuning can only offer a very limited wavelength tuning range. Thus, an adaptive laser bias control algorithm is designed to make the best of this available range to rearrange the wavelengths.

The nominal emission wavelengths for all source lasers with even spacing are denoted as vector $\vec{\lambda}_{\mathrm{nominal}}$:

$$\vec{\lambda}_{\mathrm{nominal}} = [\lambda_{n1}, \lambda_{n2}, \lambda_{n3}, \lambda_{n4}, \ldots, \lambda_{nN}]. \tag{6}$$

The current emission wavelengths from all lasers are denoted as vector $\vec{\lambda}_{\mathrm{current}}$:

$$\vec{\lambda}_{\mathrm{current}} = [\lambda_{c1}, \lambda_{c2}, \lambda_{c3}, \lambda_{c4}, \ldots, \lambda_{cN}]. \tag{7}$$

As the goal is to separate them evenly with the nominal spacing, the target wavelengths are denoted as vector $\vec{\lambda}_{\mathrm{goal}}$:

$$\vec{\lambda}_{\mathrm{goal}} = \vec{\lambda}_{\mathrm{nominal}} + \lambda_g = [\lambda_{g1}, \lambda_{g2}, \lambda_{g3}, \lambda_{g4}, \ldots, \lambda_{gN}] \tag{8}$$

where $\lambda_g$ is a constant that minimizes the distance between vector $\lambda_g$ and $\vec{\lambda}_{\mathrm{goal}}$. That is

$$\lambda_g = \lambda_g \text{that minimise} \left( \sqrt{\sum_{i=1}^{N} (\lambda_{gi} - \lambda_{ci})^2} \right). \tag{9}$$

Furthermore, for ensuring that the target wavelengths are reachable by thermal tuning, the final wavelength results $\lambda_{\mathrm{new}}$ will be

$$\lambda_{\mathrm{new}.i} = \begin{cases} \lambda_{gi}, \text{if } |\lambda_{gi} - \lambda_{ci}| \leq \text{Tuning range (TR)} \\ \lambda_{ci} + \mathrm{TR}, \quad \text{if } \lambda_{gi} - \lambda_{ci} > \mathrm{TR} \\ \lambda_{ci} - \mathrm{TR}, \quad \text{otherwise.} \end{cases} \tag{10}$$

However, as shown in the top row of Eq. (10), for some lasers, the tunable range is not fully used. The residual wavelength tunable range, denoted as $\lambda_{\mathrm{res}}$, can still be further used to optimize the wavelength spacing

$$\lambda_{\mathrm{res}.i} = \mathrm{TR} - |\lambda_{\mathrm{new}.i} - \lambda_{ci}| \quad . \tag{11}$$

Therefore, a second stage of bias tuning is designed to fully utilize these residual tunable ranges. The flow chart shown in Fig. 5 illustrates a single iteration of rearranging the wavelength

TABLE I
POWER DISSIPATIONS FOR PROPOSED SYSTEM AND CONVENTIONAL SYSTEM

| MIMO DWDM Transceiver | | Conventional DWDM Transceiver | |
|---|---|---|---|
| Devices | Power (mW/Ch) | Devices | Power (mW/Ch) |
| Laser + Driver | $161 + 500$ [23] | Laser + Driver | $132 + 500$ |
| 9-tap Decoder [a] | $9 \times 13.2$ [24] | TEC | 1125 |
| ADC & DSP for updating taps [b] | $(79 + 300)/40$ [25], [26] | | |
| Micro Processor (Bias Control) | 50 [27] | Micro Processor | 50 |
| $2.8 \times (\mathrm{PIN} + \mathrm{TIA})$ [c] | $2.8 \times 100$ [28] | PIN+TIA | 100 |
| CDR | 72 [29] | CDR | 72 |
| Total | 1191 mW/Ch | Total | 1979 mW/Ch |

[a] Nine taps are required for the signals to be decoded in the worst case scenario.
[b] The ADC/DSP is used to update taps for every decoder and can be shared by all MIMO decoders on different time slots through electrical switching.
[c] As in average, each transmitter need 2.8 receiver channels to decode.

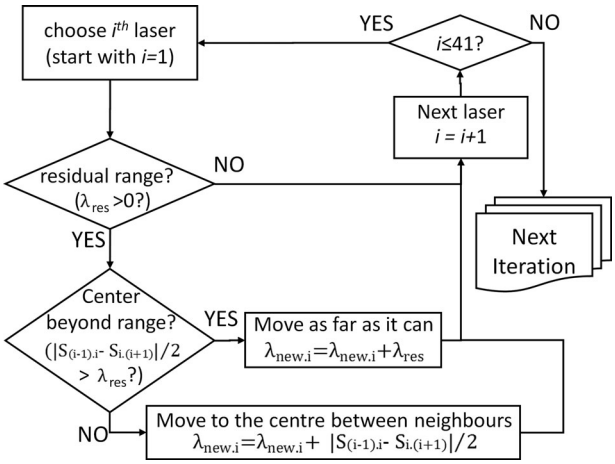


Fig. 5. A single iteration of the second stage bias tuning, where $S_{i,j}$ represents the spacing between laser $i$'s and laser $j$'s wavelengths, $(S_{i,j} = \lambda_i - \lambda_j)$.

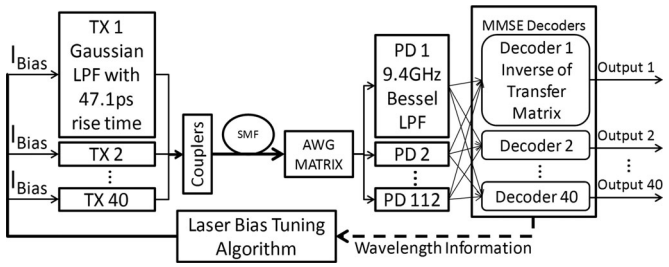


Fig. 6. Schematic diagram of simulated system.

space using the residual tunable range. 100 iterations are executed to make sure almost all residual tunable ranges are used to optimize the channel spacing. All lasers are checked in every loop. Once the range of wavelengths feasible for a given laser is determined, the system seeks to shift the wavelength to be equidistant between the two neighboring wavelengths. If this center position is beyond the possible wavelength range of the laser, the system shifts the wavelength as much as it can. It should be noted that, when the signals are de-multiplexed by a cyclic AWG, this involving the calculation of the spacing between the first and the last channels, a full spectrum range (FSR) should be subtracted from the results

$$\begin{cases} S_{1.40} = S_{1.0} = \lambda_1 - \lambda_{40} + \mathrm{FSR} \\ S_{40.1} = S_{40.41} = \lambda_{40} - \lambda_1 - \mathrm{FSR}. \end{cases} \tag{12}$$

## IV. SIMULATION OF THE PROPOSED SYSTEM

A simulation is carried out to validate the performance of this tuning algorithm. As shown in Fig. 6, there are 40 lasers whose nominal emission wavelengths are evenly distributed from 1525 to 1565 nm, which is equal to the working window of most EDFAs. The lasers nominally operate at 25 °C and their emission wavelength may vary with either the ambient temperature or the bias current. The ambient temperature is allowed to drift within a 50 °C range and the lasers' bias currents are set between 40 and 200 mA, which is feasible for most practical DFB lasers. The wavelength drift rate and the thermal tuning rate are set to be 0.1 nm/°C and 1 GHz/mA, respectively [30]. The modulated waveform of a 12.5 Gb/s NRZ signal is modeled by a Gaussian low pass filter (LPF) with a 20%–80% rise time of 47.1 ps. The data pattern is a pseudo random binary sequence (PRBS) with a length of $2^{31}$–1. Every channel's PRBS is generated from a unique seed for the sake of de-correlation between data sequences.

At the receiver, an AWG with 112 output channels is used as the de-multiplexer. The proposed channel profile in Section II is emulated by a second order Gaussian filter with a 3 dB bandwidth of 0.65 nm. The AWG outputs are detected by photodiodes incorporating a 4th order Bessel LPF with a 3 dB bandwidth of 9.4 GHz. The parameters in both the Gaussian LPF and the Bessel LPF agree with those chosen by the IEEE802.3ae 10 Gb/s Ethernet Task Force [31].

The simulation starts by assuming a random distribution of laser temperatures with associated drift wavelengths. The bias tuning algorithm then adapts the laser drive currents step by step to optimize the channel spacing, as shown in Fig. 7(a). Fig. 7(b) shows how the power penalties of the spectral channels are minimized as optimization progresses.

In reality, the laser temperatures vary with time. Fig. 8 shows how the algorithm continuously adjusts the lasers' bias currents

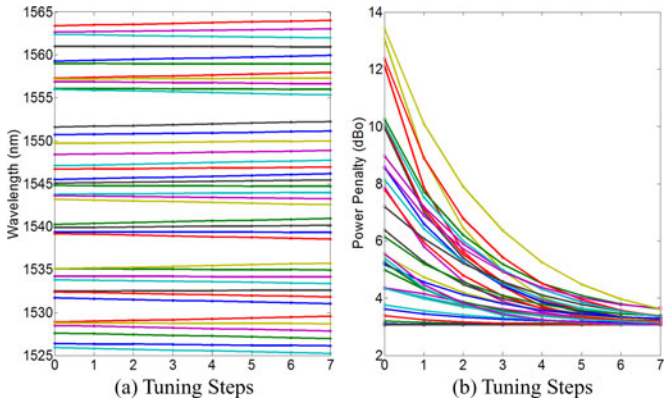


Fig. 7. (a) Wavelengths over the tuning process. (b) Power penalties of MMSE decoders for each channel. The colours of the channels here correspond to the colours in Fig. 7(a).

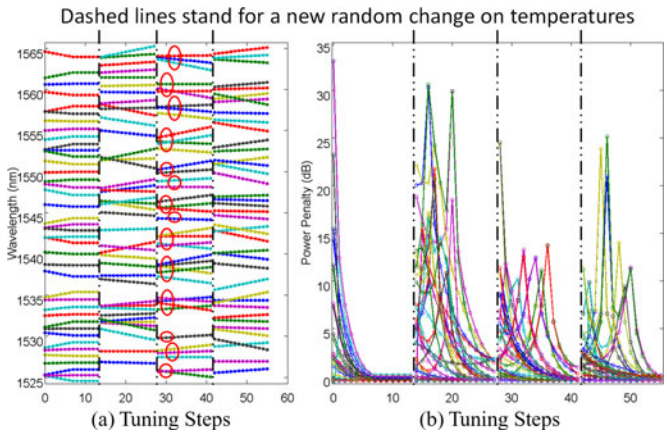


Fig. 8. (a) Wavelength variation under multiple changes of the temperatures. (b) Power penalty of the worst decoder varies during the tuning process.

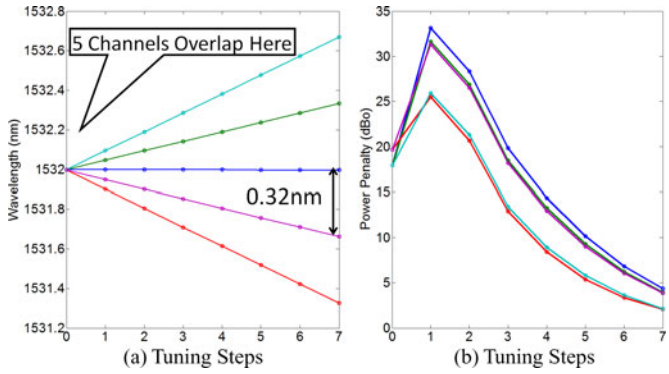


Fig. 9. Power penalties in the worst case scenario.

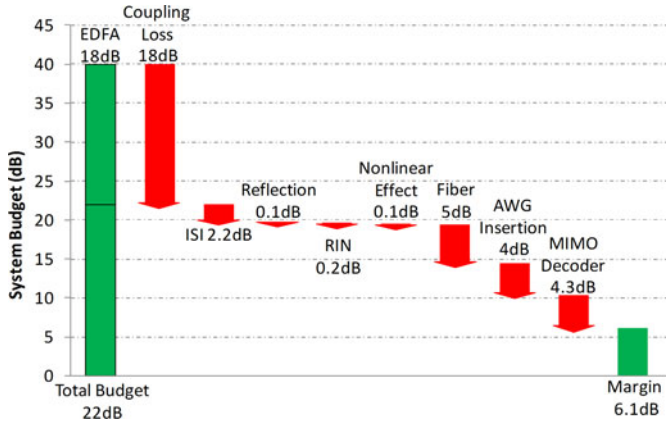


Fig. 10. Power budget of the system.

to adapt the varying temperature and recover the system. Each discontinuity in the wavelength indicates a random and instant change of the temperature in every laser. As can be seen, every time when the temperatures of the source lasers change, the emission wavelengths are rearranged which makes some channels move close to the others, causing significant increases of their decoded output power penalties. However, as the bias control algorithm progresses, all channel spacings are optimized and hence power penalties of their decoders are minimized. It should be noted that in reality the rate of the temperature change can be neglected compared to that of the algorithm response. Therefore, as the algorithm is running repeatedly, the power penalty of the MMSE decoder can be kept at a reasonably low level (see Fig. 8).

However, this random-temperature-drift model cannot represent all possible cases of the system, so a worst case scenario has been designed as shown in Fig. 9. This assumes an initial temperature distribution which causes the output of five lasers to overlap at exactly 1532 nm. Only five lasers are considered in this scenario as given the 50 °C temperature range, a laser's emission wavelength can only drift within $\pm 2.5$ nm, which covers at most 4 neighboring lasers' wavelengths. Thus, 5 is the largest number of lasers that can emit at a single wavelength. On the other hand, from the decoding algorithm's viewpoint, a 40-channel system can always be seen as a few parallel channel groups (red circles in Fig. 8(a), which only contain no more than 5 lasers, other channels not contributing to performance penalties. Fig. 9(a) shows that even in the worst case, the bias tuning algorithm can separate the wavelengths by 0.32 nm spacing, ensuring successful data transmission. Also, by using 14 receiver channels which is 2.8 times of the number of transmitters, the power penalty of the worst channel's MMSE decoder is recovered to less than 4.3 dB (see Fig. 9(b)). However, any decoding system with fewer than 14 receiver channels will lead to a decoding penalty of more than 5 dB, caused by more noise amplifications in every MMSE decoder.

The worst case power budget and system margin for the decoders are shown in Fig. 10. The total budget is calculated by assuming a 0 dBm laser output and a receiver with a sensitivity of $-22$ dBm, which are indicated in the line card standard Telcordia GR-253 OC192 LR2 [32]. A 20 dB gain from a post-fiber EDFA, whose noise figure is 2 dB, is used to compensate the loss caused by the couplers and the fibers. As can be seen from Fig. 10, even under the worst case scenario, the system still has more than 6 dB margin.

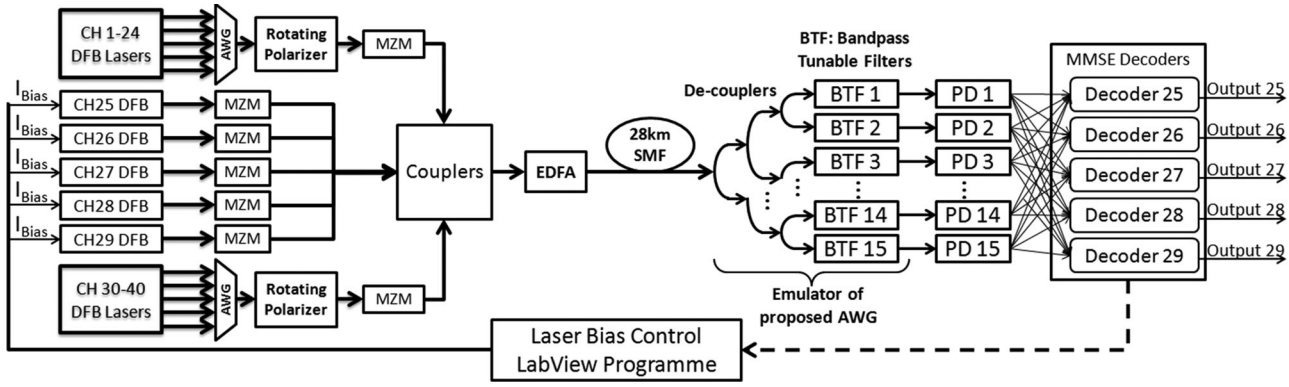


Fig. 11. Schematic diagram of the experimental setup.

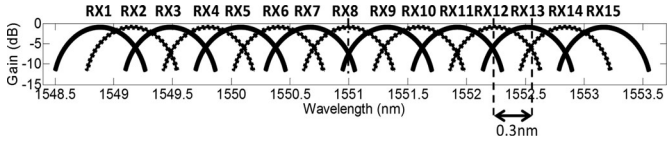


Fig. 12. AWG filters' (receiver channels) center positions.

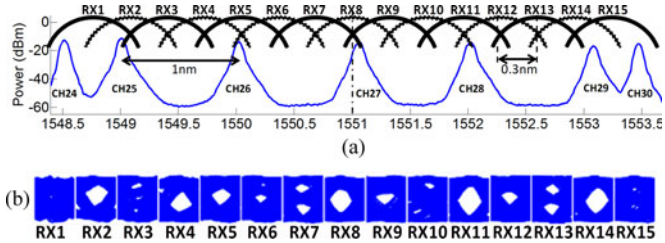


Fig. 13. OSA trace (a) and directly received eye diagrams (b) from all receiver channels before temperature (wavelength) drift. All lasers in Ch25∼29 are operating at 25 °C and all lasers' bias currents are 100 mA.

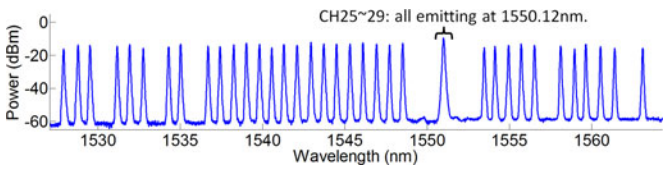


Fig. 14. OSA trace of 40 channels, the temperatures of Ch25∼29 are adjusted so that they all emit at the same wavelength (temperatures are 45, 36, 28, 17 and 5 °C, respectively). All lasers' bias currents are still 100 mA.

## V. Experimental Results

### A. Setup of the Demonstration System

An experiment is performed to assess the system performance under the worst case scenario. As shown in Fig. 11, 40 standard DFB lasers with nominal emission wavelengths between 1525 and 1565 nm with 125 GHz nominal spacing are deployed. Temperature controllers for transmitter channels 25–29 are used to set the temperatures to the worst case distribution, causing these five laser emission wavelengths to overlay each other. Temperatures in all the other 35 lasers are left uncontrolled. The bias current of each laser starts at 100 mA and they all can be tuned from 45 to 205 mA with a thermal tuning rate of around 1 GHz/mA, resulting in a tuning range of 1.3 nm. For the sake of the assessment (as in practice lasers should be direct modulated), the source lasers for channels 25–29 are independently modulated by Mach–Zehnder modulators with de-correlated 12.5 Gb/s NRZ pseudo random data patterns of $2^{31}$–1 length. The lasers for channels 1–24 and channels 30–40 are modulated by two separate Mach–Zehnder modulators after being coupled by an AWG and the polarization of these lasers is rotated mechanically to ensure all sources are modulated and interfering with the central five lasers under test. The outputs from these three groups of lasers are then coupled together by three-stage couplers and amplified by an EDFA and then transmitted through 28 km of SMF-28 fiber.

At the receiver end, the optical signal is first recorded by an optical spectrum analyzer. Once the wavelength information is obtained, it is fed back to a LabView program running on a PC to run the bias tuning algorithm. Then the program controls the programmable current sources to adjust the laser drive currents to optimize the channel spacing. Then the signal is de-multiplexed by two cascaded tunable band pass filters (each with 0.8 nm bandwidth). The central positions of these filters are adjusted to emulate an AWG with 0.65 nm 3-dB channel bandwidth and 0.3 nm channel spacing (see Fig. 12). The resulting signal for each channel is captured by an oscilloscope and post-processed on a PC using MATLAB.

### B. Experimental Result

The experiment consists of two steps: creating a worst-case scenario temperature drift and applying the laser bias tuning algorithm. Fig. 13(a) shows the starting point where all the lasers' temperatures are nominally separated. The eye diagrams, received directly from RX channels 2, 5, 8, 11 and 14, show that they can be decoded even without MMSE decoders (see Fig. 13(b)). However, after the temperatures drift, wavelengths of channels from 25 to 29 all overlap (see Fig. 14) making successful signal decoding impossible.

Fig. 15(a) shows the spectrum after application of the tuning algorithm. The channels are now spaced at 0.31 nm. Fig. 15(b) shows the eye diagrams of the signals directly received from

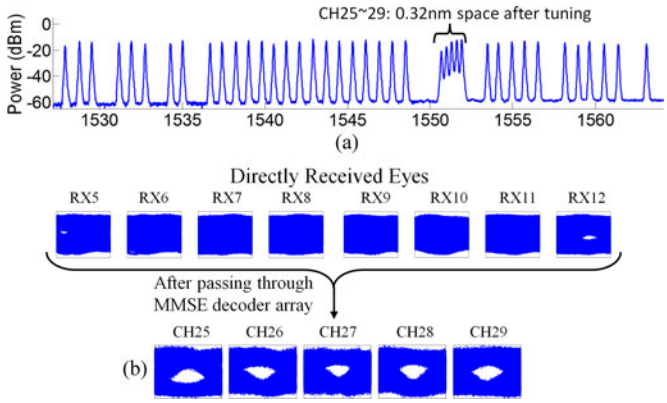


Fig. 15. (a) Optical spectra after tuning the bias currents. (The bias currents are now 50, 100, 139, 177 and 201 mA, respectively). (b) Eye diagrams after decoding.

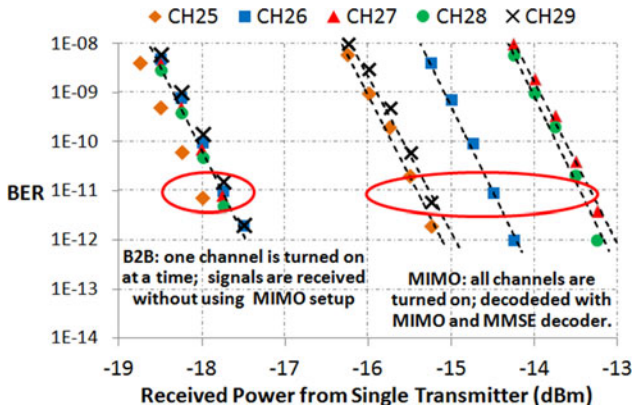


Fig. 16. BERs for ch25-ch29 after algorithm applied.

receiver channels 5–12. It can be seen that most of these non-decoded signals contain severe crosstalk. The eye diagrams of the outputs from the MMSE decoders are shown in Fig. 15(b). All channels are successfully decoded. The BER curves for channels 25–29 after tuning the bias currents, calculated using the eye diagrams decoded from the experimental results and a reference receiver with a sensitivity of –18 dBm at a BER of $10^{-12}$, are shown in Fig. 16. For each channel, the back-to-back case here is defined as only one channel is turned on and transmitted at a time and the BER is measured using the signal directly received from the photo-detector with the maximum received optical power. The MMSE decoder is used in this measurement. It can be seen that compared with the back-to-back case, when all channels are turned on and decoded with the MMSE decoder, the worst case channel has a penalty of only 4.5 dB, which is very close to the result from simulation.

## VI. Conclusion

In this paper, we propose and demonstrate a novel MIMO DWDM system using standard uncooled and independent DFB lasers. This design allows the emission wavelength of each independent laser to continuously drift with temperature. A feedback based laser bias control algorithm is introduced to constantly optimize the wavelength spacing between adjacent lasers. A MIMO receiver based on an AWG with more receiver channels than transmitters followed by a MMSE decoder array is used to ensure the signal can always be detected and recovered even with severe crosstalk.

A comprehensive simulation in MATLAB is shown in order to investigate the performance of the system under different temperature scenarios. A scenario with five lasers all emitting at the same wavelength is considered to be the worst case within the given temperature range. In this worst case scenario, there is a 4.3 dB power penalty from the worst MMSE case decoder leading to at least 6 dB margin in the proposed system.

In order to validate the simulation result, we demonstrate a 40 channel uncooled DWDM system with the temperatures from five neighboring lasers the same as the worst case scenario. After applying the laser bias tuning algorithm, all channels are successfully decoded and the power penalty of the worst channel's MMSE decoder is only 4.5 dB. In summary this MIMO WDM system is predicted to reduce the power consumption by 40%.

## References

[1] (Jun. 2014). Cisco White Paper. *Cisco visual networking index: Forecast and methodology, 2013–2018*. [Online]. Available: http://www.cisco.com/c/en/us/ solutions/ collateral/ service-provider/ ip-ngn-ip-next-generation-network/white_paper_c11–481360.html

[2] C. A. Brackett, "Dense wavelength division multiplexing networks: Principles and applications," *IEEE J. Sel. Areas Commun.*, vol. 8, no. 6, pp. 948–964, Aug. 1990.

[3] B. Mukherjee, "WDM optical communication networks: Progress and challenges," *IEEE J. Sel. Areas Commun.*, vol. 18, no. 10, pp. 1810–1824, Oct. 2000.

[4] N. S. Bergano, "Wavelength division multiplexing in long-haul transoceanic transmission systems," *IEEE/OSA J. Lightw. Technol.*, vol. 23, no. 12, pp. 4125–4139, Dec. 2005.

[5] A. N. Pilipetskii, "High-capacity undersea long-haul systems," *IEEE J. Sel. Topics Quantum Electron.*, vol. 12, no. 4, pp. 484–496, Jul./Aug. 2006.

[6] (2000). Cisco White Paper. *Introduction to DWDM for metropolitan networks*. [Online]. Available: http://www.abrconsulting.com /White%20Papers/dwdm.pdf

[7] A. Bianco, T. Bonald, D. Cuda, and R. Indre, "Cost, power consumption and performance evaluation of metro networks," *IEEE/OSA J. Opt. Commun. Netw.*, vol. 5, no. 1, pp. 81–91, Jan. 2013.

[8] C.-H. Lee, S.-M. Lee, K.-M. Choi, J.-H. Moon, S.-G. Mun, K.-T. Jeong, J. H. Kim, and B. Kim, "WDM-PON experiences in Korea [Invited]," *J. Opt. Netw.*, vol. 6, pp. 451–464, 2007.

[9] A. Banerjee, Y. Park, F. Clarke, H. Song, S. Yang, G. Kramer, K. Kim, and B. Mukherjee, "Wavelength-division-multiplexed passive optical network (WDM-PON) technologies for broadband access: A review [Invited]," *J. Opt. Netw.*, vol. 4, pp. 737–758, 2005.

[10] R. Huelsermann, K. Grobe, and D. Breuer, "Cost and performance evaluation of WDM-based access networks," presented at the Nat. Fiber Opt. Eng. Conf., Anaheim, CA, USA, Mar. 2013, Paper NTh3F.4.

[11] R. S. Tucker, "Green optical communications—Part I: Energy limitations in transport," *IEEE J. Sel. Topics Quantum Electron.*, vol. 17, no. 2, pp. 245–260, Mar./Apr. 2011.

[12] J. L. Wei, J. D. Ingham, D. G. Cunningham, R. V. Penty, and I. H. White, "Performance and power dissipation comparisons between 28 Gb/s NRZ, PAM, CAP and optical OFDM systems for data communication applications," *IEEE/OSA J. Lightw. Technol.*, vol. 30, no. 20, pp. 3273–3280, Oct. 15 2012.

[13] J. Baliga, K. Hinton, and R. S. Tucker, "Energy consumption of the internet," presented at the Joint Conf. Opt. Int. Australian Conf. Opt. Fibre Technol., Melbourne, Australia, Jun. 2007.

[14] Y. J. Chen, "Low cost WDM technology for emerging telecommunications applications," presented at the Lasers Electro-Opt. Soc. Ann. Meet., San Francisco, CA, USA, Nov. 10–13, 1997, Paper ThN2.

[15] A. Davies, S. Fan, R. V. Penty, and I. H. White, "Active wavelength control of tunable lasers for use in uncooled WDM systems," presented at the Conf. Lasers Electro-Opt., Baltimore, MD, USA, Jun. 6–6, 2003, Paper CThW6.
[16] T. Sakamoto, S. Nobuo, S. Koike, K. Hadama, and K. Naoya, "4 channel $\times$ 10 Gbit/s optical module for CWDM links," in Proc. 54th Electron. Component Technol. Conf., Jun. 1–4, 2004, vol. 1, pp. 1024–1028.
[17] M. Roppelt, F. Pohl, K. Grobe, M. Eiselt, and J.-P. Elbers, "Tuning methods for uncooled low-cost tunable lasers in WDM-PON," presented at the Nat. Fiber Opt. Eng. Conf., Los Angeles, CA, USA, Mar. 6–10, 2011, Paper NTuB1.
[18] S. H. Lee, A. Wonfor, R. V. Penty, I. H. White, G. Busico, R. Cush, and M. Wale, "Uncooled DWDM transmission system using tunable laser sources with anti-mode-hop control protocol," presented at the Photon. Conf., Arlington, VA, USA Oct. 9–13, 2011, Paper TuE2.
[19] S. H. Lee, A. Wonfor, R.V. Penty, I. H. White, G. Busico, R. Cush, and M. Wale, "Self-configuring athermal tunable DS-DBR laser for passive optical networks," presented at the Conf. Lasers Electro-Opt./Quantum Electron. Laser Sci. Conf., San Jose, CA, USA, May 2010, Paper CWN5.
[20] L. Chrostowski, C. Chih-Hao, and C. J. Chang-Hasnain, "Injection-locked 1.55-$\mu$m tunable VCSEL for uncooled WDM transmitter applications," *Photon. Technol. Lett.*, vol. 16, no. 3, pp. 888–890, Mar. 2004.
[21] I. H. White, J. D. Ingham, S. H. Lee, and R. V. Penty, "Uncooled dense WDM," in *Proc. Commun. Photon. Conf.*, Guangzhou, China, Nov. 2012, Paper AF3C.1.
[22] J. Ingham, S. Lee, R. Penty, I. White, and D. Cunningham, "100 Gb/s uncooled WDM system using conventional WDM components and advanced receiver signal processing," presented at the Eur. Conf. Exhib. Opt. Commun., Amsterdam, The Netherlands, Sep. 16–20, 2012, Paper P4.09.
[23] (May 2003). *Datasheet for MAX3935 EAM Driver*. [Online]. Available: http://datasheets.maximintegrated.com/en/ds/MAX3935.pdf
[24] Y. Tomita, M. Kibune, J. Ogawa, W. W. Walker, H. Tamura, and T. Kuroda "A 10 Gb/s receiver with equalizer and on-chip ISI monitor in 0.11 $\mu$m CMOS," in Proc. Symp. VLSI Circuits Dig. Tech. Papers, Jun. 17–19, 2004, pp. 202–205.
[25] E. Z. Tabasy, A. Shafik, L. Keytaek, S. Hoyos, and S. Palermo, "A 6b 10GS/s TI-SAR ADC with embedded 2-tap FFE/1-tap DFE in 65nm CMOS," in *Proc. VLSI Circuits Symp.*, Jun. 12–14, 2013, pp. C274–C275.
[26] (2014). Xilinx, Inc. *Power Efficiency for Xilinx 7 series*. [Online]. Available: http://www.xilinx.com/products/technology/power/index.htm
[27] (Jun. 2013). Datasheet for DS4830 Optical Microcontroller. [Online]. Available: http://datasheets.maximintegrated.com/en/ds/DS4830.pdf
[28] (Sep. 2012). Datasheet for JDSU 1310/1550 nm XFP ROSA. [Online]. Available: http://www.jdsu.com/ProductLiterature/rxpmgrtl097-ds-oc-ae.pdf
[29] J. Savoj and B. Razavi, "A 10-Gb/s CMOS clock and data recovery circuit with a half-rate linear phase detector," *IEEE J. Solid-State Circ.*, vol. 36, no. 5, pp. 761–768, May 2001.
[30] M. Funabashi, H. Nasu, T. Mukaihara, T. Kimoto, T. Shinagawa, T. Kise, K. Takaki, T. Takagi, M. Oike, T. Nomura, and A. Kasukawa, "Recent advances in DFB lasers for ultradense WDM applications," *IEEE J. Sel. Topics Quantum Electron.*, vol. 10, no. 2, pp. 312–320, Mar./Apr. 2004.
[31] *IEEE Standard for Information technology– Local and Metropolitan Area Networks—Part 3*, IEEE 802.3ae, 2002.
[32] (Oct. 2009). *Synchronous optical network (SONET) transport systems: Common generic criteria, GR-253*, [Online]. Available: http://telecom-info.telcordia.com/site-cgi/ido/docs.cgi?ID=294058922 SEARCH&DOCUMENT=GR-253;

**Jiannan Zhu** received the B.Sc. degree in electrical and electronic engineering from the Huazhong University of Science and Technology, Wuhan, China, in 2011. He is currently working toward the Ph.D. degree at the Centre for Photonic Systems, Engineering Department, University of Cambridge, Cambridge, U.K. His current research interests include datacoms and passive optical networks.

**Jonathan D. Ingham** (M'99) received the M.A. degree from the University of Cambridge, Cambridge, U.K., and the Ph.D. degree from the University of Bristol, Bristol, U.K. He read electrical and electronic engineering at Imperial College London, and received the Ph.D. degree from the University of Bristol before joining the Department of Engineering, University of Cambridge, Cambridge, U.K. He has authored more than 70 peer-reviewed papers in leading journals and conferences.

**Johannes Benedikt von Lindeiner** received the M.Eng. and M.Res. degrees from UCL, London, U.K., in 2010 and 2011, respectively. He is currently working toward the Ph.D. degree with the Centre for Photonic Systems, Electrical Engineering Division, University of Cambridge, Cambridge, U.K. He is a Peer Reviewer for the JOURNAL OF LIGHTWAVE TECHNOLOGY. He received the Grand Prize for the Corning Outstanding Student Paper Competition held at OFC in 2014.

**Adrian Wonfor** (M'02) received the B.Sc. degree in physics from the University of Bath, Somerset, U.K., in 1992. He is a Senior Research Associate at the Centre for Photonic Systems, Engineering Department, University of Cambridge, Cambridge, U.K. He is the author or coauthor of more than 100 publications and is the holder of several patents.

**Richard V. Penty** (SM'10) received the Ph.D. degree from the University of Cambridge, Cambridge, U.K., in 1989. He is currently working toward the Master of Sidney Sussex College. He was a Science and Engineering Research Council Information Technology Fellow at the University of Cambridge, where he is currently a Professor of Photonics. He has held academic posts at the University of Bath, Bath, U.K., and the University of Bristol, Bristol, U.K. He is the author or coauthor of more than 700 publications. He is the Editor-in-Chief of the Institution of Engineering and Technology, *Optoelectronics Journal* and the Founder of Zinwave, Ltd.

**Ian H. White** (S'82–M'83–SM'00–F'05) received the B.A. and Ph.D. degrees from the University of Cambridge, Cambridge, U.K., in 1980 and 1984, respectively. He is currently the Deputy Vice-Chancellor at the Master of Jesus College, van Eck Professor of Engineering, and the Head of Photonics Research, Department of Engineering, University of Cambridge. He was a Member of the Board of Governors of the IEEE Photonics Society (2008–2012) and is an Editor-in-Chief of Electronics Letters. He has published in excess of 800 publications and holds 28 patents.